AC Loss Reduction in HTS Coil Windings Coupled with an Iron Core

Yue Wu, Jin Fang, Naoyuki Amemiya, Rodney A. Badcock, *Senior Member, IEEE*, Nicholas J. Long, and Zhenan Jiang, *Senior Member, IEEE*

***Abstract*—Rapid-cycling synchrotron (RCS) magnets based on a superferric design consist of high temperature superconducting (HTS) coil windings coupled with iron cores. However, the presence of iron cores significantly increases AC loss in HTS coil windings, making AC loss reduction a critical issue for applying HTS technology in RCSs. Enlarging the distance between iron cores and coil windings may reduce AC loss. In addition, magnetic materials with different saturation magnetic fields also may influence AC loss in HTS coil windings coupled with iron cores. To investigate the distance dependence, AC losses of 1DPC (double pancake coil)-, 2DPC-, 4DPC-, and 8DPC assemblies with various distances are simulated using the 3D *T-A* homogenization method with/without an iron core. Two magnetic materials with different saturation magnetic fields are chosen as the iron core to evaluate AC loss in HTS coil assemblies. The results show that the AC loss values in HTS coil assemblies coupled with the iron core decrease significantly with growing distance. For a given distance and current, when the iron core has a lower saturation field, the AC loss values of the 4DPC assembly are smaller than those with a higher saturation field.**

***Index Terms*—AC loss, iron core, superconducting coils, 3D *T-A* homogenization method.**

I. Introduction

As the next generation accelerators for cancer treatment, rapid-cycling synchrotrons (RCSs) are desired to be built on the base of high temperature superconducting (HTS) coil windings to minimize magnet size and reduce electricity consumption [1]. The proposed superferric magnets are based on HTS coil windings coupled with iron cores [2]-[4]. Due to the presence of iron cores, a significant AC loss increase in HTS coil windings was observed, and hence AC loss becomes one of the main concerns of superferric magnets and new generation RCS application [5]-[9].

More recently, in our previous work [9], we carried out AC loss simulations on HTS coil windings coupled with an iron core using the 3D *T-A* homogenization method [10]-[12]. Results showed that the AC loss in the 8DPC (double pancake coil) assembly coupled with the iron core is more than one order larger than that without the iron core [9]. Several studies have reported that the AC loss of HTS coil windings shows dependence on the number of stacked coils and the inner diameter of coils [13]-[15]. As the schematic depicted in Fig.1, the distance (d) is defined as the gap from the outer diameter of the iron core to the inner diameter of the coil assembly. Therefore, the distance, d, can vary with different inner diameters (d_1) of coils and AC loss reduction might be achieved by increasing this distance by weakening the influence of the iron core. In addition, magnetic materials with different saturation magnetic fields also resulted in different AC losses in HTS coil windings [16]-[19]. However, no systematic work has been carried out for HTS coil windings coupled with an iron core to explore AC loss dependence on the number of stacked coils, d values, and saturation fields of the iron core.

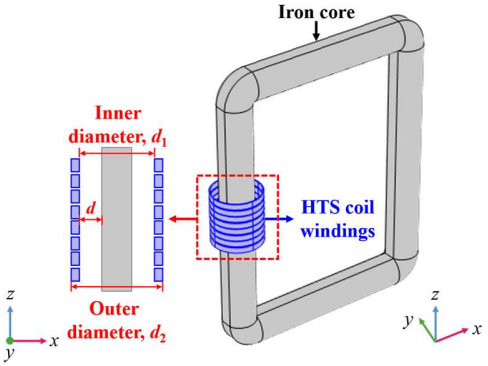

Fig. 1. Schematic of RE(BCO) coil windings coupled with an iron core.

In this work, AC loss simulations were carried out to study loss dependence on the stacked number of DPCs, d values, and the saturation magnetic field of the iron core by using the 3D *T-A* homogenization method. AC loss in the 1DPC-, 2DPC-, 4DPC-, and 8DPC assemblies wound with 4 mm-wide Shanghai Superconductor wires with and without the iron core having

Manuscript received November 10, 2022. This work was supported in part by the New Zealand MBIE under Contract No. RTVU1707 and in part by the SSIF "Advanced Energy Technology Platforms" under Contract No. RTVU2004. Yue Wu acknowledges financial supports from the CSC and the CSC/Victoria University of Wellington Scholarship. *(Corresponding author: Zhenan Jiang and Jin Fang.)*

Y. Wu is with the School of Electrical Engineering, Beijing Jiaotong University, Beijing 100044, China, and also with the Robinson Research Institute, Victoria University of Wellington, 69 Gracefield Road, Lower Hutt 5011, New Zealand (e-mail: wuyue_1018@126.com).

J. Fang is with the School of Electrical Engineering, Beijing Jiaotong University, Beijing, 100044, China. (e-mail: jfang@bjtu.edu.cn).

N. Amemiya is with the Graduate School of Engineering, Kyoto University, Kyoto 615-5120, Japan. (e-mail: amemiya.naoyuki.6a@kyoto-u.ac.jp).

R. Badcock, N. Long and Z. Jiang are with the Robinson Research Institute, Victoria University of Wellington, 69 Gracefield Road, Lower Hutt 5011, New Zealand (e-mail: rod.badcock@vuw.ac.nz; nick.long@vuw.ac.nz; zhenan.jiang@vuw.ac.nz).

Color versions of one or more of the figures in this paper are available online at http://ieeexplore.ieee.org.

Digital Object Identifier will be inserted here upon acceptance.

various d values are compared when they carry different transport currents. Moreover, magnetic materials with different saturation magnetic fields are considered to investigate the influence of saturation field on AC loss characteristics of the coil windings.

II. Numerical Method

A. T-A Formulation

In the *T-A* formulation [10], the current vector potential $\boldsymbol{T}$ is defined in the superconducting wire, while the magnetic vector potential $\boldsymbol{A}$ is employed in the entire model. $\boldsymbol{T}$ and $\boldsymbol{A}$ are defined by

$$\boldsymbol{J} = \nabla \times \boldsymbol{T} \tag{1}$$

$$\boldsymbol{B} = \nabla \times \boldsymbol{A} \tag{2}$$

here $\boldsymbol{J}$ is the current density and $\boldsymbol{B}$ is the magnetic flux density.

The governing equations of the $\boldsymbol{T}$ and $\boldsymbol{A}$ formulations are:

$$\nabla \times \left(\rho_{\mathrm{HTS}} \nabla \times \boldsymbol{T} \right) = -\frac{\partial \boldsymbol{B}}{\partial t} \tag{3}$$

$$\nabla \times \left(\frac{1}{\mu_0 \mu_{\mathrm{r}}} \nabla \times \boldsymbol{A} \right) = \boldsymbol{J} \tag{4}$$

where μ_0 is the vacuum permeability, μ_{r} is the relative permeability of the magnetic material. μ_{r} values of iron cores are obtained from *B-H* curves of 'Silicon Steel NGO 50PN290' and 'Silicon Steel NGO 35JN200' in COMSOL Multiphysics shown in Fig. 2.

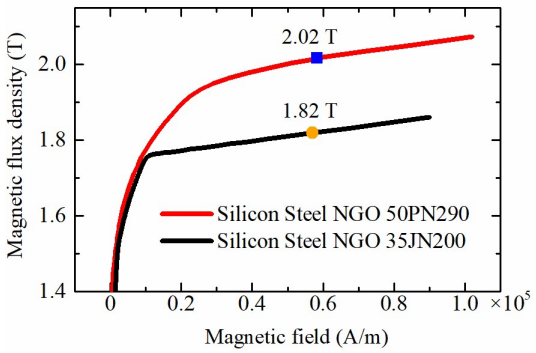

Fig. 2. *B-H* curves of Silicon Steel NGO 50PN290 and Silicon Steel NGO 35JN200 used in the simulation models.

The resistivity of the superconductor, ρ_{HTS}, is derived from the *E-J* power law:

$$\rho_{\mathrm{HTS}} = \frac{E_{\mathrm{c}}}{J_{\mathrm{c}}(\boldsymbol{B})} \left| \frac{\boldsymbol{J}}{J_{\mathrm{c}}(\boldsymbol{B})} \right|^{n-1} \tag{5}$$

where $E_{\mathrm{c}} = 10^{-4}$ V/m and $n = 17$ [9].

To describe the $J_{\mathrm{c}}(\boldsymbol{B})$ relationship of the superconductor, the modified Kim model [19] is adopted:

$$J_{\mathrm{c}}(\boldsymbol{B}) = J_{\mathrm{c0}} \left(1 + \frac{k^2 B_{\mathrm{para}}^2 + B_{\mathrm{perp}}^2}{B_0^2}\right)^{-\alpha} \tag{6}$$

where J_{c0}, k, B_0, and α are fitting parameters obtained from critical current measurements under applied magnetic fields. In this work, $J_{\mathrm{c0}} = 4.815 \times 10^{10}$ A/m^2, $k = 0.24$, $B_0 = 0.03$, and $\alpha = 0.23$. B_{para} and B_{perp} are the parallel and perpendicular magnetic field components to the HTS layer.

B. 3D T-A Homogenization Method

The main specifications of the coated conductor, DPC, and iron core can be found from Table I.

TABLE I
SPECIFICATIONS OF COATED CONDUCTOR, DPC AND IRON CORE

Coated conductor	Manufacturer	Shanghai Superconductor Co.
	Substrate	Hastelloy
	Width (mm)	4.0
	Total thickness (μm)	85.0
	Thickness of superconducting layer (μm)	1
	$I_{\mathrm{c,\ self\text{-}field}}$ (A)	192.6
DPC (each)	Inner diameter (mm)	35.0
	Outer diameter (mm)	36.5
	Total height (mm)	9.0
	Turn number	10
Iron core	Materials	Silicon Steel NGO 50PN290/35JN200
	Outer diameter of cross-section (mm)	22
	Dimensions (mm)	Rectangular (93×211)

To simulate coil assemblies using the 3D *T-A* homogenization method, the scaled current density in the homogenous bulk is defined to calculate $\boldsymbol{A}$ as:

$$\boldsymbol{J}_{\mathrm{bulk}} = \boldsymbol{J} \cdot \frac{d}{t_{\mathrm{wire}}} \tag{7}$$

here J_{bulk} is the current density of the homogeneous bulk, d is the thickness of the superconducting layer, and t_{wire} is the total thickness of the coated conductor.

The transport current in each DPC is imposed by setting boundary conditions for every surface of the equivalent homogeneous bulk [9]. Since the homogeneous bulk is supposed to carry the summation of currents of all turns, Dirichlet boundary conditions are applied to the top and bottom surfaces of the bulk to handle such transport current [21]:

$$I = (T_1 - T_2) \cdot d \tag{8}$$

where T_1 and T_2 are the values of $\boldsymbol{T}$ on the top and bottom surfaces.

In addition, Neumann boundary conditions are applied to the internal and external surfaces to fulfil the definition as [12], [22]:

$$\frac{\partial (n_{\mathrm{x}} \cdot T_{\mathrm{x}} + n_{\mathrm{y}} \cdot T_{\mathrm{y}} + n_{\mathrm{z}} \cdot T_{\mathrm{z}})}{\partial \boldsymbol{n}} = 0 \tag{9}$$

where n_{x}, n_{y}, and n_{z} are the local normal components of the x-, y-, and z axes. $\boldsymbol{n}$ is a unitary vector perpendicular to the HTS layer in the coordinate, as presented in Fig. 1.

The 3D *T-A* homogenization method has been validated by comparing simulated and measured results of a double pancake coil [9].

This article has been accepted for publication in IEEE Transactions on Applied Superconductivity. This is the author's version which has not been fully edited and content may change prior to final publication. Citation information: DOI 10.1109/TASC.2023.3246944

III. Results and Discussion

A. HTS Coil Assemblies with Different d Values Coupled with the Iron Core

The inner diameters (d_1) and outer diameters (d_2) of different DPCs used in this work are listed in Table II. Each DPC maintains the same turn number. Distances (d) are also given in Table II. As shown in Fig. 1, the right limb of the iron core is far away from the 4DPC assembly to eliminate its influence on AC loss, and thus, loss in coil windings is only influenced by d.

TABLE II
Parameters of different DPCs and distances

	#1	#2	#3	#4	#5
Inner diameter, d_1 (mm)	35	45.5	52.5	59.5	70
Outer diameter, d_2 (mm)	36.5	47	54	61	71.5
Distance, d (mm)	6.5	11.75	15.25	18.75	24

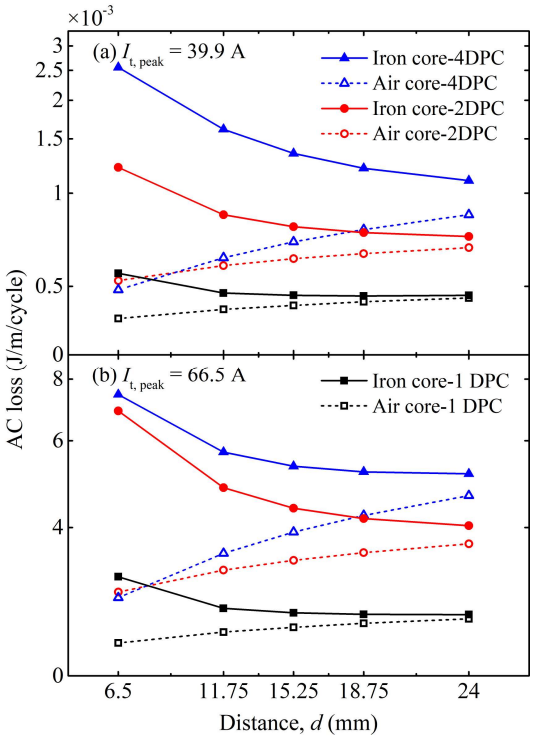

Fig. 3. AC loss results of the 1DPC-, 2DPC-, and 4DPC assemblies with/without the iron core at different d values (f = 13.96 Hz): (a) $I_{t,\,peak}$ = 39.9 A, (b) $I_{t,\,peak}$ = 66.5 A.

In Fig. 3, AC loss results of the 1DPC-, 2DPC-, and 4DPC assemblies with/without the iron core at f = 13.96 Hz, $I_{t,\,peak}$ = 39.9 A and 66.5 A, are plotted as a function of d. With increasing d, AC loss in the DPC assemblies with the iron core decreases, whereas AC loss in all assemblies increases without the iron core. Compared with the coil assemblies that have a smaller inner diameter without the iron core, the coil assemblies with a larger inner diameter experience a larger perpendicular magnetic field component (B_{perp}), which increases the AC loss. By and large, the difference in AC loss values between coil assemblies with and without the iron core becomes much smaller with growing d for all coil assemblies. For a given d and current, the differences in AC loss values of coil assemblies with and without iron core increase with the number of stacked DPCs. At $I_{t,\,peak}$ = 39.9 A, comparing the 4DPC and 1DPC assemblies with/without the iron core, the AC losses are increased by 136% and 33.4% at d = 6.5 mm, while 25.3% and 1.89% at d = 24 mm. At $I_{t,\,peak}$ = 66.5 A, for the 4DPC assembly with/without the iron core, the AC loss values are increased by 88.3% at d = 6.5 mm and 10.2% at d = 24 mm. As shown above, the growth rate of AC loss in the 4DPC assembly coupled with the iron core over that without the iron core weakens with increasing transport current.

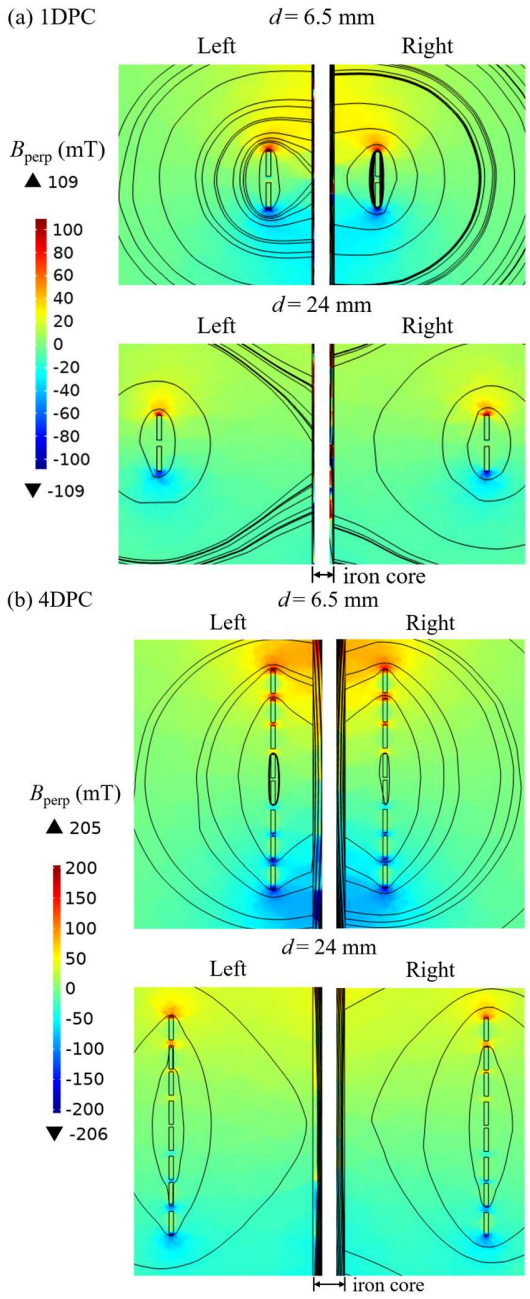

Fig. 4. Magnetic flux lines and perpendicular magnetic field distributions in the left and right cross sections of the 1DPC and 4DPC assemblies with the iron core at d = 6.5 mm and d = 24 mm (f = 13.96 Hz, $I_{t,\,peak}$ = 39.9 A, t = 3/4 cycle): (a) the 1DPC assembly, (b) the 4DPC assembly.

This article has been accepted for publication in IEEE Transactions on Applied Superconductivity. This is the author's version which has not been fully edited and content may change prior to final publication. Citation information: DOI 10.1109/TASC.2023.3246944

Fig. 4 presents magnetic flux lines and B_{perp} distributions in the left and right cross sections of the 1DPC and 4DPC assemblies with the iron core at f = 13.96 Hz, $I_{t,\,peak}$ = 39.9 A, and t = 3/4 cycle, when d = 6.5 mm and 24 mm. The magnetic flux lines distribute asymmetrically around the 1DPC and 4DPC assemblies owing to the non-axisymmetric characteristic of the analyzed geometry. For the 1DPC assembly, the area filled with large B_{perp} at d = 6.5 mm is slightly larger than that at d =24 mm, explaining only a minor difference in AC loss results between these two cases shown in Fig. 3 (a). For the 4DPC assembly at d = 6.5 mm, if we look at its upper half, large B_{perp} has penetrated the upper end part of its end disc and two inner discs. Since the geometry of the 4DPC assembly is symmetrical along the z-axis, the B_{perp} distribution in its bottom half keeps the same as its upper half with an opposite magnetic field direction. However, when d = 24 mm, the penetration region of the 4DPC assembly significantly shrinks, further interpreting the results in Fig. 3 (a) that increasing d can effectively reduce the AC loss in the 4DPC assembly.

Fig. 5 plots magnetic flux lines and perpendicular magnetic field distributions in the left and right cross sections of the 4DPC assembly without and with the iron core at f = 13.96 Hz, $I_{t,\,peak}$ = 39.9 A, and t = 3/4 cycle, when d = 24 mm. Although similar B_{perp} distributions are observed when the 4DPC assembly with and without the iron core, the region filled with large B_{perp} is slightly larger in the case with the iron core (Fig. 5(b)) than the case without the iron core (Fig.5 (a)), explaining the AC loss results shown in Fig. 3(a).

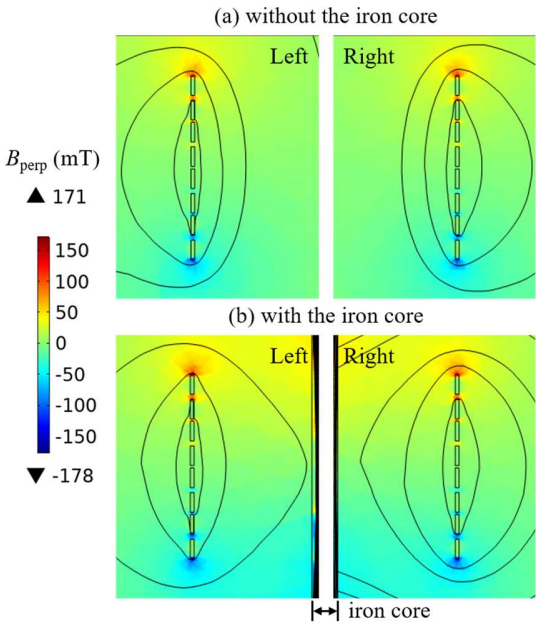

Fig. 5. Magnetic flux lines and perpendicular magnetic field distributions in the left and right cross sections of the 4DPC assembly with and without the iron core at d = 24 mm (f = 13.96 Hz, $I_{t,\,peak}$ = 39.9 A, t = 3/4 cycle).

Fig. 6 is replotted from the AC loss results shown in Fig. 3. Fig.6 shows the AC loss in the 1DPC-, 2DPC-, and 4DPC assemblies coupled with the iron core ($Q_{Iron\ core}$) normalized by the AC loss in the coil windings without the iron core ($Q_{Air\ core}$), plotted as a function of d, at f = 13.96 Hz, $I_{t,\,peak}$ = 39.9 A and 66.5 A. At $I_{t,\,peak}$ = 39.9 A, the $Q_{Iron\ core}/Q_{Air\ core}$ values of the 1DPC and 2DPC assemblies quickly converge to 1 with increasing d compared with the case of the 4DPC assembly. This can also be explained by Fig. 4. For the 1DPC assembly, there is no significant difference in the B_{perp} distribution between d = 6.5 mm and d = 24 mm. However, for the 4DPC assembly at d = 24 mm, the area filled with large B_{perp} greatly shrinks in most discs compared with the case for d = 6.5 mm, making a big difference in AC loss values. At $I_{t,\,peak}$ = 66.5 A, a larger $Q_{Iron\ core}/Q_{Air\ core}$ value is expected for the 4DPC assembly. However, the result shows a smaller $Q_{Iron\ core}/Q_{Air\ core}$ value and also a faster trend to approach 1 with increasing d values compared with the case for $I_{t,\,peak}$ = 39.9 A. We attribute the result to the saturation of the iron core. For the case of the 4DPC assembly with the iron core carrying $I_{t,\,peak}$ = 66.5 A, the ability of the iron core to attract magnetic flux lines weakens due to its saturation.

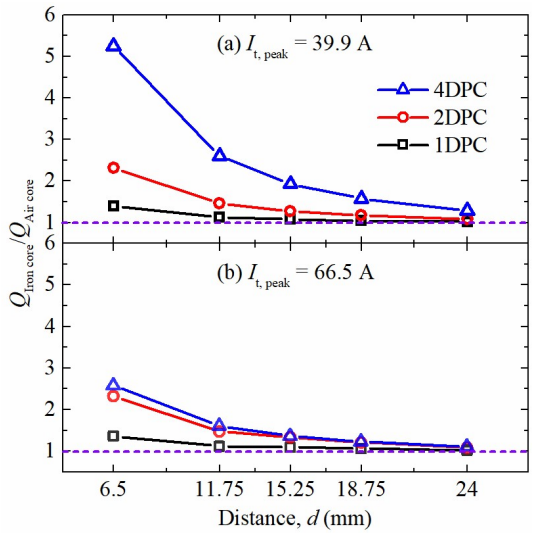

Fig. 6. $Q_{Iron\ core}/Q_{Air\ core}$ results of 1DPC-, 2DPC- and 4DPC assemblies with/without the iron core at different d values (f = 13.96 Hz): (a) $I_{t,\,peak}$ = 39.9 A, (b) $I_{t,\,peak}$ = 66.5 A. Here $Q_{Iron\ core}$ means AC loss with the iron core while $Q_{Air\ core}$ means AC loss without the iron core.

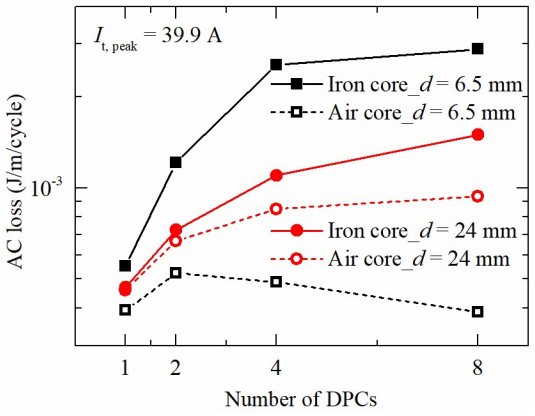

Fig. 7. AC loss results of different number of DPCs with/without the iron core at d = 6.5 mm and d = 24 mm (f = 13.96 Hz, $I_{t,\,peak}$ = 39.9 A).

Fig. 7 shows the AC loss of the DPC assemblies with/without the iron core at f = 13.96 Hz, $I_{t,\,peak}$ = 39.9 A plotted as a function of the number of stacked DPCs at d = 6.5 mm and d = 24 mm.

At d = 6.5 mm without the iron core, AC loss in the coil assemblies per unit length at a given current increases with growing number of DPCs until it reaches a peak value and then decreases. However, at d = 24 mm without the iron core, AC losses in DPC assemblies still increase with growing number of DPCs. The different tendencies for d = 6.5 mm and 24 mm should be due to the difference in the coil geometry [13]. In all DPC assemblies, for both d = 6.5 mm and d = 24 mm, the AC loss difference between the coil assemblies with and without the iron core increases with growing DPC number. Moreover, the difference in AC losses for DPC assemblies at d = 24 mm becomes much smaller than that at d = 6.5 mm. At d = 6.5 mm, the presence of the iron core dramatically increases the large B_{perp} area in coil assemblies, leading to a significant loss increase. However, at d = 24 mm, the iron core loses some of its capability to attract flux lines, causing small difference in AC loss values between coil assemblies with and without the iron core.

B. Iron Cores with Different Saturation Magnetic Fields

In Fig.2, the saturated magnetic flux density of 'Silicon Steel NGO 50PN290' is around 2 T, while 1.75 T for 'Silicon Steel NGO 35PN200'. For the 4DPC assembly coupled with the iron core, at d = 6.5 mm, f = 13.96 Hz, and $I_{t,\,peak}$ = 39.9 A, the maximum magnetic flux densities in the iron core using 50PN290 and 35JN290 are 2.02 T and 1.82 T, respectively. As marked in Fig. 2, the iron core with a high saturation field begins to saturate in this case because its magnetic flux density just reaches the saturated value. In comparison, the iron core with a low saturation field is in a fully saturated state.

Fig. 8 compares AC loss results in the 4DPC assembly with different d values with/without different iron cores at f = 13.96 Hz and $I_{t,\,peak}$ = 39.9 A. The AC loss values of the 4DPC assembly decrease with growing d when coupled with the iron core. However, when the iron core has a lower saturation field, the AC loss values of the 4DPC assembly are smaller than those with a higher saturation field. This should be caused by the difference in the relative permeability values for the two cases due to saturation. Although the AC loss in the 4DPC assembly with the iron core decreases by using a low saturation field iron core, the difference between the results without and with the iron core is still significant.

Fig. 9 presents $Q_{Iron\ core}/Q_{Air\ core}$ results versus different d values of the 4DPC assembly coupled with different iron cores at f = 13.96 Hz, when $I_{t,\,peak}$ = 39.9 A and 66.5 A. When the iron core has a low saturation field, the $Q_{Iron\ core}/Q_{Air\ core}$ values are smaller than those with a high saturation field at both currents. At d =6.5 mm and $I_{t,\,peak}$ = 66.5 A, the maximum magnetic flux density in the iron core is 2.06 T for 50PN290, and 1.87 T for 35JN290. It means both iron cores are saturated at the current. In the saturated condition, relative permeability of the iron cores decreases compared to un-saturated condition. Therefore, the AC loss differences of the 4DPC assembly between with and without iron cores cannot increase further. The results clearly show that AC loss of the HTS assembly coupled with the iron core is influenced by the saturation field of the iron core. It is worth noting that the $Q_{Iron\ core}/Q_{Air\ core}$ value gradually approaches 1 when increasing the distance between the iron core and the 4DPC assembly at $I_{t,\,peak}$ = 66.5 A.

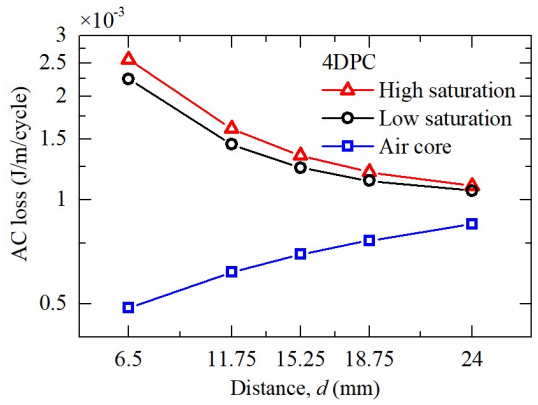

Fig. 8. AC loss results of the 4DPC assembly with/without different iron cores at different d values (f = 13.96 Hz, $I_{t,\,peak}$ = 39.9 A).

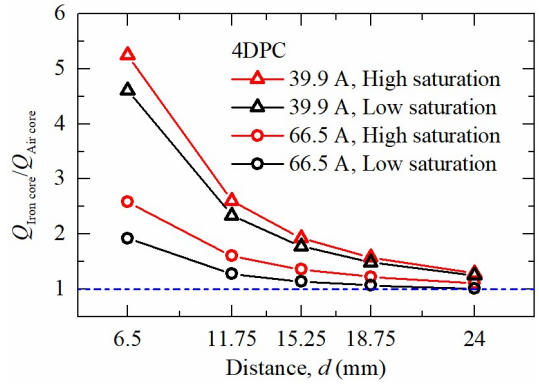

Fig. 9. $Q_{Iron\ core}/Q_{Air\ core}$ results of the 4DPC assembly coupled with different iron cores at different d values (f = 13.96 Hz).

IV. Conclusion

To reduce AC loss in HTS coil windings coupled with iron cores, systematic simulations were carried out using the 3D *T-A* homogenization method to investigate AC loss dependence on the number of stacked DPCs, the d values, and the saturation magnetic field of the iron core. Moreover, AC losses of the 1DPC-, 2DPC-, 4DPC-, and 8DPC assemblies, wound with 4 mm-wide Shanghai Superconductor wires, were calculated with different distance values and with/ without iron cores.

The results showed a remarkable AC loss reduction caused by enlarging the distance in all DPC assemblies. In addition, the magnetic field perpendicular to the coil surface is greatly decreased with growing distance, which implies that increasing the distance weakens the influence of the iron core on AC loss in the coil assemblies.

For the 4DPC assembly, the $Q_{Iron\ core}/Q_{Air\ core}$ values decrease with increasing coil current for all distance values due to the saturation of the iron core. For a given distance and current, decreasing the saturation field of the iron core decreases the $Q_{Iron\ core}/Q_{Air\ core}$ values for the 4DPC assembly. It was shown that AC loss in the HTS assemblies cannot increase dramatically after the iron core has been magnetized to the saturated state.

REFERENCES

[1] H. Piekarz, B. Claypool, S. Hays, M. Kufer, V. Shiltsev, and A. Zlobin, "Fast cycling HTS based superconducting accelerator magnets: feasibility study and readiness demonstration program driven by neutrino physics and muon collider needs," *the Proceeding of Snowmass 2021*, arXiv preprint arXiv:2203.06253, Mar. 2022.

[2] R. Gupta, M. Anerella, J. Cozzolino, J. Escallier, G. Ganetis, A. Ghosh, M. Harrison, A. Marone, J. Muratore, J. Schmalzle, W. Sampson, and P. Wanderer, "Status of high temperature superconductor magnet R&D at BNL," *IEEE Trans. Appl. Supercond.*, vol. 14, no. 2, pp. 1198-1201, Jun. 2004.

[3] H. Piekarz, J. Blowers, S. Hays, and V. Shiltsev, "Design, construction, and test arrangement of a fast-cycling HTS accelerator magnet," *IEEE Trans. Appl. Supercond.*, vol. 24, no. 3, Jun. 2014, Art. no. 4001404.

[4] Y. Chen, Z. Du, W. Wu, B. Wu, X. Ou, T. Yang, and S. Zheng, "Design, fabrication and test of a 1.5 T cryogen-free HTS dipole magnet for the heavy ion spectrometer," *IEEE Trans. Appl. Supercond.*, vol. 32, no. 6, Sept. 2022, Art. no. 4001205.

[5] L. Lai, C. Gu, T. Qu, M. Zhang, Y. Li, R. Liu, T. Coombs, and Z. Han, "Simulation of AC loss in small HTS coils with iron core," *IEEE Trans. Appl. Supercond.*, vol. 25, no. 3, Jun. 2015, Art. no. 4700905.

[6] Y. Sogabe, M. Yasunaga, Y. Fuwa, Y. Kuriyama, T. Uesugi, Y. Ishi, and N. Amemiya, "AC Losses in HTS coils of superferric dipole and combined-function magnets for rapid-cycling synchrotrons," *IEEE Trans. Appl. Supercond.*, vol. 29, no. 5, Jun. 2019, Art. no. 5900505.

[7] X. Xu, Z. Huang, X. Huang, L. Hao, J. Zhu, B. Shen, W. Li, J. Jiang, M. Wang, and Z. Jin, "Numerical study on AC loss of an HTS coil placed on laminated silicon steel sheets with distorted AC transport currents," *IEEE Trans. Appl. Supercond.*, vol. 30, no. 4, Jun. 2020, Art. no. 4702105.

[8] Y. Li, Y. Sogabe, M. Yasunaga, Y. Fuwa, Y. Ishi, and N. Amemiya, "Reduction of ac loss in HTS coils of superferric magnets for rapid-cycling synchrotrons by changing cross-section of coils and iron yoke geometry," *IEEE Trans. Appl. Supercond.*, vol. 30, no. 4, Jun. 2020, Art. no. 4700905.

[9] Y. Wu, X. Li, R. Badcock, N. Long, N. Amemiya, J. Fang, and Z. Jiang, "AC loss simulation in HTS coil windings coupled with an iron core," *IEEE Trans. Appl. Supercond.*, vol. 32, no. 6, Sept. 2022, Art. no. 4701505.

[10] H. Zhang, M. Zhang M, and W. Yuan, "An efficient 3D finite element method model based on the T–A formulation for superconducting coated conductors," *Supercond. Sci. Technol*., vol. 30, no. 2, Dec. 2016, Art. no. 024005.

[11] V. M. R. Zermeno, A. B. Abrahamsen, N. Mijatovic, B. B. Jensen, and M. P. Serensen, "Calculation of alternating current losses in stacks and coils made of second generation high temperature superconducting tapes for large scale applications," *J. Appl. Phys.*, vol. 114. no. 17, pp. 1-19, Nov. 2013.

[12] C. R. Vargas-Llanos, F. Huber, N. Riva, M. Zhang, and F. Grilli, "3D homogenization of the T-A formulation for the analysis of coils with complex geometries," *Supercond. Sci. Technol.*, vol. 35, no. 12, Oct. 2022, Art. no. 124001.

[13] E. Pardo, J. Šouc, and J. Kováč1, "AC loss in ReBCO pancake coils and stacks of them: modelling and measurement," *Supercond. Sci. Technol.*, vol. 25, no. 3, Jan. 2012, Art. no. 035003.

[14] Y. Sogabe, Z. Jiang, S. Wimbush, N. Strickland, M. Staines, N. Long, and N. Amemiya, "AC loss characteristics in REBCO coil assemblies with different geometries and conductors," *IEEE Trans. Appl. Supercond.*, vol. 28, no. 3, Apr. 2018, Art. no. 4700105.

[15] W. Song, Z. Jiang, M. Staines, R. A. Badcock, and J. Zhang, "Design of a single-phase 6.5 MVA/25 kV superconducting traction transformer for the Chinese Fuxing high-speed train," *Int. J. Electr. Power Energy Syst.*, vol. 119, Jun. 2020, Art. no. 105956.

[16] O. Tsukamoto, H. Nakayama, S. Odaka, M. Ciszek, S. Hahakura, M. Ueyama, K. Ohmatsu, and D. Miyagi, "Transport current losses in Ho-BaCuO-123 coated conductors with a Ni-alloy substrate," *Phy. C: Supercond. its Appl.*, vol. 426-431, pp. 1290-1294, Oct. 2005.

[17] J. Knott, and J. Moscrop, "Increasing energy efficiency of saturated-core fault current limiters with permanent magnets," *IEEE Trans. Magn.*, vol. 49, no. 7, pp. 4132–4136, Jul. 2013.

[18] Y. Jia, M. Ainslie, D. Hu, and J. Yuan, "Numerical simulation and analysis of a saturated-core-type superconducting fault current limiter," *IEEE Trans. Appl. Supercond.*, vol. 27, no. 4, Jun. 2017, Art. no. 5600805.

[19] S. You, D. Miyagi, R. Badcock, N. Long, and Z. Jiang, "Experimental and numerical study on AC loss reduction in a REBCO coil assembly by applying high saturation field powder-core flux diverters," *Cryogenics*, vol. 124, Jun. 2022, Art. no. 103466.

[20] Y. B. Kim, C. F. Hempstead, and A. R. Strnad, "Critical persistent currents in hard superconductors," *Phys. Rev. Lett.*, vol. 9, pp. 306–312, 1962.

[21] E. Berrospe-Juarez, F. Trillaud, V. Zermeño, and F. Grilli, "Advanced electromagnetic modeling of large-scale high-temperature superconductor systems based on H and T-A formulations," *Supercond. Sci. Technol.*, vol. 34, no. 4, Feb. 2021, Art. no. 044002.

[22] E. Berrospe-Juarez, V. Zermeño, F. Trillaud, and F. Grilli, "Real-time simulation of large-scale HTS systems: multi-scale and homogeneous models using the T–A formulation," *Supercond. Sci. Technol.*, vol. 32, no. 6, Apr. 2019, Art. no. 065003.